# ChemComm

Check for updates

## On the factors influencing the chiroptical response of conjugated polymer thin films†

Beth Laidlaw,[a] Julien Eng, [ID][a] Jessica Wade,[bc] Xingyuan Shi, [ID][cd]
Francesco Salerno,[cd] Matthew J. Fuchter [ID][cd] and Thomas J. Penfold [ID]*[a]

We study the influence of the physical and chemical structure on the chiroptical response of fluorene-based polymeric systems, namely poly(9,9-dioctylfluorene) (PFO) and the donor–acceptor type copolymer poly(9,9-dioctylfluorene-*alt*-benzothiadiazole) (F8BT). We reveal the significance of electric-magnetic coupling, at both short (molecular-level) and intermediate (delocalised over multiple polymer chains) length scales, on the magnitude of the dissymmetry. These findings provide a framework for the design of new materials with an enhanced chiroptical response.

Chirality is a fundamental symmetry property, which can play a defining role in a broad range of areas. Recently, it has gained significant interest in optoelectronic applications, such as organic light-emitting diodes (OLEDs) and organic photodetectors, where the use of a chiral material in the active layer enables the emission or detection of circularly polarised (CP) light, respectively.[1] Interest in the development of chiral organic materials for CP-OLEDs[2] has led to a variety of approaches being pursued. These can be broadly grouped into two classes; small-molecule emitters[3–7] and polymer-based emitters.[8–12] The dissymmetry of the emitted light (*g*-factor) can determined by the coupling between the electric ($\mu$) and magnetic ($m$) transition dipole moments,[13] and can be expressed as:

$$g = \frac{4R}{D} = \frac{4|\mu_{ij}||m_{ij}|\cos(\tau)}{|\mu_{ij}|^2 + |m_{ij}|^2} \qquad (1)$$

where $R$ is the rotatory strength and $D$ is the overall transition strength composed of the sum of $|\mu_{ij}|^2$ and $|m_{ij}|^2$. $i$ and $j$ refer to the

initial and final states involved in the electronic transition. $\tau$ is the angle between $\mu$ and $m$. In the visible regime the wavelength of light is much larger (hundreds of nanometres) than the typical size of a molecule (tens of Angström) and therefore the electric dipole approximation is valid (see Section S1, ESI†) meaning that the electric-magnetic coupling (natural optical activity, eqn (1)) is small. The magnetic transition dipole only becomes significant for dipole forbidden transitions or when $kr > 1$,[14] *i.e.* high photon energies when $k = 2\pi/\lambda$ becomes large or if the exciton size, which influences the electron separation occurring in $r$ becomes $\sim$ the wavelength of light (see ESI†).

When considering transitions allowed within the electric dipole approximation, eqn (1) indicates that *g*-factors are limited to values of $\sim 10^{-3}$.[15] Larger dissymmetric responses can be achieved for molecules that make use of electric-dipole forbidden transitions, including chiral lanthanide complexes ($g \sim 1.4$).[16] However, owing to their small $\mu$, they typically demonstrate low emission cross sections, which results in luminescence quantum yields too low for display applications. While efforts continue to address the trade-off between luminescence quantum yield and dissymmetry,[15] it remains a challenge to identify highly emissive organic molecules with excellent CP characteristics.

An alternative approach to sizeable CP response is based upon non-intrinsic light-matter interactions observed in systems with long-range structural chirality, such as in chiral nematic (cholesteric) liquid crystals (LC).[17] Here dissymmetry is determined by Bragg-type circular selective reflections off the thin film and not the intrinsic polarisation of light at the site of emission. The magnitude of this phenomenon is therefore sensitive to the pitch and thickness of cholesteric LC films.[18]

Currently, organic systems generating the largest dissymmetric response in the solid state (*g*-factors up to $\sim$ 1) are conjugated polymers, especially amongst the polyfluorene class.[11] It has been proposed that this strong CP luminescence occurs due to structural chirality.[8,12,19] However, recent works[9,20] have indicated that long-range structural chirality only dominates the chiroptical response when an alignment

*[a] Chemistry – School of Natural and Environmental Sciences, Newcastle University, Newcastle upon Tyne, NE1 7RU, UK. E-mail: tom.penfold@ncl.ac.uk*

*[b] Department of Materials, Imperial College London, South Kensington Campus, London, SW7 2AZ, UK*

*[c] Centre for Processable Electronics, Imperial College London, South Kensington Campus, London, SW7 2AZ, UK*

*[d] Department of Chemistry, Molecular Sciences Research Hub, Imperial College London, White City Campus, 82 Wood Lane, London W12 0BZ, UK*
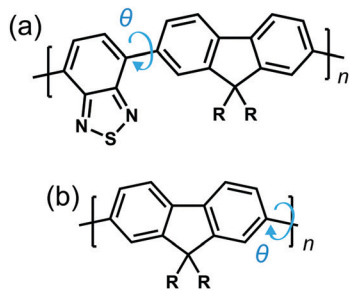
Fig. 1 Structures of the simplified models of (a) F8BT and (b) PFO. R are $C_8H_{17}$ side chains, however herein, R represents methyl groups. $n$ represents the number of repeat units and the arrows indicate the twist angle ($\theta$) between adjacent repeat units.

layer is used to template molecular packing of polymer chains at or beyond the mesoscale. Highly dissymmetric emission from non-aligned thin polymer films (*i.e.*, those where the film thickness is considerably less than those at which this structural chiroptical phenomena manifest) suggests that intrinsic CP emission may play a significant role.[20,21]

To explore the origins of the strong chiroptical response of polymer-based systems, we turn to time-dependent density functional theory (TDDFT), within the approximation of the CAM-B3LYP exchange and correlation functional[22] (see ESI†). We consider the influence of four variables on the $g$-factor; chemical composition, the intramolecular twist angle ($\theta$) between adjacent repeat units, the number of monomers ($n$) a single oligomer chain is made of and the role of interchain (intermolecular) coupling. Two model fluorene-based systems were studied (Fig. 1), namely PFO and F8BT. To reduce computational expense, we focus on low numbers of monomer repeat units (often $n = 2$) and the $C_8H_{17}$ side chains were replaced with methyl groups, noting that it has been shown that the side chains can play an important role in controlling chiral induction in thin films.[23] The lowest excited state of PFO corresponds to the $\pi \rightarrow \pi^*$ transition. The calculated $S_1$ state of an isolated oligomer ($\theta = 40°$, $n > 4$) is 318 nm (see Fig. S1, ESI†). For F8BT ($\theta = 40°$, $n > 3$), the lowest transition exhibits a charge-transfer character between the F8 and BT units and the calculated $S_1$ state of the isolated oligomer is 427 nm (see Fig. S1, ESI†). These are in reasonable agreement with the lowest absorption bands, 375 nm and 475 nm, measured for PFO and F8BT, respectively.[20]

Fig. 2a shows the $g$-factor (calculated using eqn (1)) of the $S_1$ state of isolated PFO and F8BT oligomers as a function of $n$ with a fixed $\theta = 40°$, close to the optimised twist angle for F8BT[9] and the glassy-phase PFO.[24] In both cases, the $g$-factor initially increases before a plateau is reached at $n = 3$ and $n = 5$ for PFO and F8BT, respectively. This behaviour bears some resemblance to the work of Greenfield *et al.*,[25] who reported a plateau associated maximum length over which the exciton can delocalise for a given configuration. Here the plateau is reached earlier for PFO ($n = 3$) than F8BT owing to a larger exciton binding energy of PFO compared to F8BT (F8BT = 0.2 eV,[9] PFO = 0.3 eV[26]). For the non-planar polymers studied in the present work, the enhanced delocalisation of F8BT[9] means that
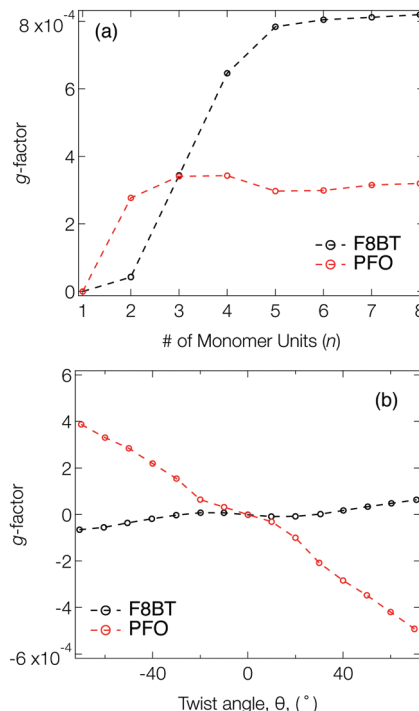


Fig. 2 (a) $g$-Factor of the $S_1$ state as a function of the number of monomer units ($n$) for PFO (red) and F8BT (black) oligomers. A fixed twist angle ($\theta = 40°$) was used throughout. (b) $g$-Factor as a function of $\theta$ for PFO (red) and F8BT (black) 2-mers ($n = 2$). The dashed line between the points are a guide for the eye.

$kr$ for F8BT will be larger than that of PFO. This results in an increase of $\boldsymbol{m}$ relative to $\boldsymbol{\mu}$, which can be seen in the decreasing $\mu^2/m^2$ ratio (Fig. S2, ESI†) and the larger predicted $g$-factors.

Fig. 2b shows the $g$-factor as a function of $\theta$ for PFO and F8BT 2-mers (*i.e.*, $n = 2$). In both cases the $g$-factor increases with the magnitude of $\theta$, and its sign is determined by direction, which indicates that the handedness/sign of the CP response can be controlled by the direction of the cumulative twist along the polymer backbone. The impact of $\theta$ is more pronounced for PFO because (i) the ratio $\mu^2/m^2$ is considerably smaller in PFO for $\theta > 30°$ (Fig. S3a, ESI†) and (ii) the angle $\tau$ between $\boldsymbol{\mu}$ and $\boldsymbol{m}$ (Fig. S3b, ESI†) deviates more from 90°. In general, $\boldsymbol{\mu}$ and $\boldsymbol{m}$ decreases as $\theta$ increases and this reduction is greater for F8BT as the coupling strength between the (intrachain) donor and acceptor decreases as $\theta$ approaches orthogonality. This leads to a larger relative decrease in $\boldsymbol{m}$ compared to $\boldsymbol{\mu}$ and therefore an increase in the ratio $\mu^2/m^2$ (Fig. S3a, ESI†). Whilst this is unfavourable for achieving high $g$-factors, it is offset by the increase in $\cos(\tau)$. The same is not observed for PFO as we are considering the $\pi-\pi^*$ transition of the homopolymer. As $\theta$ increases, the delocalised exciton exhibits an increased $\boldsymbol{m}$ compared to $\boldsymbol{\mu}$, reflected in the ratio $\mu^2/m^2$ (Fig. S3a, ESI†). The angle $\tau$ between $\boldsymbol{m}$ and $\boldsymbol{\mu}$ increases, which supports the enhancement of the $g$-factor.

The above examples have shown how, for isolated oligomers, the $g$-factor depends on the extent of exciton delocalisation, which is ultimately related to the validity of the dipole

**Fig. 3** (a) *g*-Factor as a function of the distance between the centre-of-mass of each chain in a dimer of PFO (red) and F8BT (black) 2-mers (*n* = 2, *θ* = 40°). The angle between the two polymer chains in the dimer (*φ*) was fixed at 2°. The dashed line is a fit using $d^{-3}$ illustrating a decay in the dissymmetry consistent with a reduction in the exciton coupling. (b) *g*-Factor as a function of the angle (*φ*) between the two polymer chains (*n* = 2, *θ* = 40°) in the dimer. The distance between the 2-mers was fixed at 6 Å.



**Fig. 4** (a) Schematic of two polymer chains and the coordinates (*d* and *φ*) manipulated in Fig. 3. (b) Density difference of the lowest exciton of a F8BT dimer model illustrating the electron density delocalised over the two chains. (c) Schematic of the effect of interacting polymer chains on the electric and magnetic transition dipole moments.

approximation (eqn (2)). Despite increasing *kr* and a larger contribution from the magnetic transition dipole moment, the calculated *g*-factors still do not exceed $10^{-3}$, *i.e.* values that are consistent with molecular-level mechanisms and considerably smaller than dissymmetry factors reported for chiral polyfluorene thin films.[9,20] Instead of isolated oligomers, we next consider the impact of inter-chain coupling on the *g*-factors.

Fig. 3a shows the dissymmetry of coupled F8BT and PFO dimers, where the geometry is determined by the centre-of-mass separation (*d*) and mutual orientation (*φ*) of the two oligomers (Fig. 4a). Initially, we fixed both the mutual orientation of the oligomers (*φ* = 10°) and the intrachain twist angle (*θ* = 40°). The method for calculating the *g*-factor for these systems is described in the ESI.† It is immediately evident that exciton delocalisation over two polymer chains, illustrated in Fig. 4b, leads to an increase in the calculated dissymmetry. At short distances (*d* < 7 Å) *g*-factors of ∼0.1 and ∼0.03 are observed for PFO and F8BT, respectively. The *g*-factor decreases as a function of $d^{-3}$ (dashed line in Fig. 3a) reflecting the decrease in exciton coupling (*V*) with distance. Fig. 3b shows the dissymmetry of the F8BT or PFO 2-mers as a function of *φ*, the angle between the oblique chains (Fig. 4b). This shows that for *φ* = 0°, the dissymmetry is similar to that of the isolated

oligomers. However, as the angle increases, a large increase in the dissymmetry is observed as the coupling between the oligomers reaches a maximum at *φ* = 10°. After this the dissymmetry decreases as *μ* increases and *m* decreases. These calculations demonstrate that like *θ* for the isolate polymers, the direction of *φ* can control the sign of the *g*-factor and overall only small angles are preferred to maximise the *g*-factor.

To understand the origin of the increase in dissymmetry shown in Fig. 3 we turn to the well-established exciton chirality model (ECM),[27,28] where the rotatory strength (*R*) for a dimer of coupled excitonic states can be defined as:

$$R = \pm \frac{1}{2}\pi\sigma \boldsymbol{d}_{kl} \cdot (\boldsymbol{\mu}_k \times \boldsymbol{\mu}_l) + \frac{1}{2}\text{Im}\{(\boldsymbol{\mu}_k \pm \boldsymbol{\mu}_l) \cdot (\boldsymbol{m}_k \pm \boldsymbol{m}_l)\} \quad (2)$$

$\boldsymbol{d}_{kl}$ is the distance vector between the two individual chromophores *k* and *l*, and *σ* is the transition energy. For the majority of coupled chromophores, one assumes that terms involving *m*, generally referred to as *μ–m* terms, are negligible because of the magnetically forbidden nature of their transition; therefore the rotatory strength can be evaluated simply by considering the coupled *μ*(*μ–μ*, first term in eqn (2)). Using this approach, the maximum value of dissymmetry is $g = \pi\sigma \boldsymbol{d}_{kl}$.[29] In the case of PFO ($S_1$ = 318 nm), the *g*-factor would only reach 0.1 (shown in Fig. 3), if $\boldsymbol{d}_{kl}$ = 100 Å, which is clearly unrealistic. This represents the breakdown of the standard ECM and emphasises that the consideration of *m* for conjugated polymer systems could be important to rationalise the magnitude of the dissymmetry observed. To explore this further we compare *R* evaluated using each component of the ECM model (eqn (2)) with those calculated using TD-DFT for a coupled dimer of a PFO 2-mer with *d* = 6 Å, *θ* = 40° and *φ* = 10°. *R* calculated using eqn (2) is $608 \times 10^{-40}$ esu² cm², which is in good agreement with the TDDFT calculation of $625 \times 10^{-40}$ esu² cm². Importantly, the relative strengths of *μ–μ* term ($368 \times 10^{-40}$ esu² cm²) and *μ–m* ($240 \times 10^{-40}$ esu² cm²) highlights that the *μ–m* coupling is important for evaluating the total rotatory strength and the *g*-factors predicted by the coupled dimer models. When *θ* = 0° (*i.e.* a planar configured polymer backbone), *R* (eqn (2)) is $853 \times 10^{-40}$ esu² cm². However, in contrast to the case of

twisted polymer backbones, the contribution of the $\mu$–$\mu$ term ($818 \times 10^{-40}$ esu$^2$ cm$^2$) dominates over $\mu$–$m$ ($35 \times 10^{-40}$ esu$^2$ cm$^2$). This highlights the role of the $\mu$–$m$ term in the generation of high $g$-factors in non-planar polymer systems.

Understanding the relative contributions of local short-range electric-magnetic coupling and longer-range structural chirality is crucial for the rational design of new materials that exhibit an intense chiroptical response. Here we demonstrate that the extension of the exciton over nearby polymer chains is critically important for enhancing the dissymmetry. By exploiting the intrinsic magnetic transition dipole moment (and therefore invoking $\mu$–$m$ coupling) arising from the helically configured polymer backbones it is possible to significantly increase the dissymmetry of dimer systems. This model may not hold in polymers which adopt a planar structure in the aggregate state as they are more likely to have negligible transition magnetic dipoles,[30] however when strong interchain excitonic coupling dominated, as recently shown in thin films of PFO[21] exceptional chiroptical response can still be achieved, but in this case it would be dominated by the $\mu$–$\mu$ coupling, as the electric-magnetic coupling negligible.

Finally, we note that the present work does not consider further exciton delocalisation over a larger stack (e.g. trimers, tetramers), nor how the delocalisation would be impacted by conformational and environmental disorder, which are likely to play a role for longer polymer chains and excitonically coupled systems comprising a larger number of chains. In addition, it is important to recognise that the polymer thin files optimised for CP-OLEDs[31] are only weakly ordered and therefore the dissymmetry will be an average over multiple orientations and configurations which emit in the film. Given that reducing the inter-chain coupling signifcnatly quenches the dissymmetry, it is possible that the overall chiroptical response would be reduced if all sites were equally likely to interact with the CP light. However, this inter-chain coupling modulates both the energy and oscillator strengths of the states involved meaning that not all sites are equally likely to absorb/emit light. To understand this, further investigations using molecular dynamics is essential and will be the focus of future work.

## Conflicts of interest

There are no conflicts to declare.

# References

1 J. R. Brandt, F. Salerno and M. J. Fuchter, *Nat. Rev. Chem.*, 2017, **1**, 0045.
2 D.-W. Zhang, M. Li and C.-F. Chen, *Chem. Soc. Rev.*, 2020, **49**, 1331–1343.
3 F. Zinna, U. Giovanella and L. D. Bari, *Adv. Mater.*, 2015, **27**, 1791–1795.
4 F. Zinna, M. Pasini, F. Galeotti, C. Botta, L. Di Bari and U. Giovanella, *Adv. Funct. Mater.*, 2017, **27**, 1603719.
5 J. R. Brandt, X. Wang, Y. Yang, A. J. Campbell and M. J. Fuchter, *J. Am. Chem. Soc.*, 2016, **138**, 9743–9746.
6 F. Song, Z. Xu, Q. Zhang, Z. Zhao, H. Zhang, W. Zhao, Z. Qiu, C. Qi, H. Zhang and H. H. Sung, et al., *Adv. Funct. Mater.*, 2018, **28**, 1800051.
7 Z.-P. Yan, X.-F. Luo, W.-Q. Liu, Z.-G. Wu, X. Liang, K. Liao, Y. Wang, Y.-X. Zheng, L. Zhou and J.-L. Zuo, et al., *Chem. – Eur. J.*, 2019, **25**, 5672–5676.
8 D. Di Nuzzo, C. Kulkarni, B. Zhao, E. Smolinsky, F. Tassinari, S. C. Meskers, R. Naaman, E. Meijer and R. H. Friend, *ACS Nano*, 2017, **11**, 12713–12722.
9 L. Wan, J. Wade, F. Salerno, O. Arteaga, B. Laidlaw, X. Wang, T. Penfold, M. J. Fuchter and A. J. Campbell, *ACS Nano*, 2019, **13**, 8099–8105.
10 Y. Yang, R. C. da Costa, D.-M. Smilgies, A. J. Campbell and M. J. Fuchter, *Adv. Mater.*, 2013, **25**, 2624–2628.
11 L. Wan, J. Wade, X. Shi, S. Xu, M. J. Fuchter and A. J. Campbell, *ACS Appl. Mater. Interfaces*, 2020, **12**, 39471–39478.
12 D.-M. Lee, J.-W. Song, Y.-J. Lee, C.-J. Yu and J.-H. Kim, *Adv. Mater.*, 2017, **29**, 1700907.
13 H. Tanaka, Y. Inoue and T. Mori, *ChemPhotoChem*, 2018, **2**, 386–402.
14 S. Bernadotte, A. J. Atkins and C. R. Jacob, *J. Chem. Phys.*, 2012, **137**, 204106.
15 J. Greenfield, J. Wade, J. Brandt, X. Shi, T. Penfold and M. Fuchter, *Chem. Sci.*, 2021, **12**, 8589–8602.
16 J. L. Lunkley, D. Shirotani, K. Yamanari, S. Kaizaki and G. Muller, *J. Am. Chem. Soc.*, 2008, **130**, 13814–13815.
17 N. Tamaoki, *Adv. Mater.*, 2001, **13**, 1135–1147.
18 X. Yang, X. Jin, T. Zhao and P. Duan, *Mater. Chem. Front.*, 2021, **5**, 4821–4832.
19 Y. Geng, A. Trajkovska, D. Katsis, J. J. Ou, S. W. Culligan and S. H. Chen, *J. Am. Chem. Soc.*, 2002, **124**, 8337–8347.
20 J. Wade, J. N. Hilfiker, J. R. Brandt, L. Liirò-Peluso, L. Wan, X. Shi, F. Salerno, S. T. Ryan, S. Schöche and O. Arteaga, et al., *Nat. Commun.*, 2020, **11**, 1–11.
21 L. Wan, X. Shi, J. Wade, A. J. Campbell and M. J. Fuchter, *Adv. Opt. Mater.*, 2021, 2100066.
22 T. Yanai, D. P. Tew and N. C. Handy, *Chem. Phys. Lett.*, 2004, **393**, 51–57.
23 Y. Zhao, H. Chen, L. Yin, X. Cheng, W. Zhang and X. Zhu, *Polym. Chem.*, 2018, **9**, 2295–2301.
24 X. Shi, V. Nádaždy, A. Perevedentsev, J. M. Frost, X. Wang, E. von Hauff, R. C. MacKenzie and J. Nelson, *Phys. Rev. X*, 2019, **9**, 021038.
25 J. L. Greenfield, E. W. Evans, D. Di Nuzzo, M. Di Antonio, R. H. Friend and J. R. Nitschke, *J. Am. Chem. Soc.*, 2018, **140**, 10344–10353.
26 M. A. Stevens, C. Silva, D. M. Russell and R. H. Friend, *Phys. Rev. B: Condens. Matter Mater. Phys.*, 2001, **63**, 165213.
27 N. Harada, S.-M. L. Chen and K. Nakanishi, *J. Am. Chem. Soc.*, 1975, **97**, 5345–5352.
28 T. Bruhn, G. Pescitelli, S. Jurinovich, A. Schaumlöffel, F. Witterauf, J. Ahrens, M. Bröring and G. Bringmann, *Angew. Chem., Int. Ed.*, 2014, **53**, 14592–14595.
29 B. Langeveld-Voss, R. Janssen and E. Meijer, *J. Mol. Struct.*, 2000, **521**, 285–301.
30 G. Albano, G. Pescitelli and L. Di Bari, *Chem. Rev.*, 2020, **120**, 10145–10243.
31 W. Barford and M. Marcus, *J. Chem. Phys.*, 2017, **146**, 130902.